DR2005002
Flowers et al.

## CLOSURE TEMPERATURES OF ACCESSORY MINERALS

The range of Pb diffusivity in accessory minerals provides the opportunity to reconstruct detailed thermal histories using the U-Pb isotopic system. Closure temperature (Tc) is a function of diffusivity, cooling rate, and effective diffusion radius (Dodson, 1973), and can be constrained by experimental and field-based empirical studies. The estimates below are ranges for typical diffusion radii (25-100 μm) and cooling rates (1-100 °C/m.y.). Zircon and monazite with high Tc > 1000 °C (Cherniak and Watson, 2001; Cherniak et al., 2004) are widely used to determine the timing of intrusive and metamorphic events. Titanite is increasingly recognized as a useful geochronometer because it is reactive mineral that readily grows during metamorphism (Frost et al., 2000; Aleinikoff et al., 2002), with closure temperature of 600-650 °C constrained by both experimental and field-based studies (e.g. Cherniak; 1993; Verts et al., 1996). In contrast with these minerals that commonly grow below their closure temperatures, the U-Pb systematics of apatite and rutile are typically dominated by volume diffusion (e.g. Mezger 1989; Chamberlain and Bowring, 2000). Experimental and field studies of apatite provide consistent closure temperature constraints of 450-500 °C (e.g. Cherniak et al. 1991; Krogstad and Walker, 1994; Chamberlain and Bowring, 2000). Field estimates for closure temperature in rutile are 400-450 °C (Mezger, 1989), with somewhat higher experimental determinations (Cherniak, 2000).

## ANALYTICAL METHODS

Mineral separation was carried out using standard crushing, water table, magnetic, and heavy-liquid techniques, with subsequent hand-picking of single and multigrain fractions. Titanite, apatite, and rutile grains were ultrasonically washed in high-purity water or ethanol and rinsed in acetone, followed by a second washing in high-purity water and rinsing with double-distilled acetone. Selected rutile fractions were abraded without pyrite and washed briefly with dilute $HNO_3$. Sample spiking with a mixture of $^{205}Pb$-$^{233}U$-$^{235}U$ was followed by dissolution in 29*M* HF (titanite, rutile) or 12*M* HCl (apatite), conversion to 6*M* HCl, and chemical separation of U and Pb using HBr-HCl anion-exchange chemistry. Pb and U analyses were carried out on the Massachusetts Institute of Technology VG Sector 54 mass spectrometer. Pb isotopic ratios were measured by peak jumping using an axial ion-counting Daly detector or dynamically with Faraday cups and the Daly detector. U was measured as an oxide in static mode on three Faraday cups. Details regarding isotopic ratio corrections are provided in Table DR1[1].

The incorporation of significant common Pb of uncertain isotopic composition into apatite and rutile during crystallization, resulting in low ratios of radiogenic Pb to common Pb, is a particularly acute problem for U-Pb age determination in young, less radiogenic samples. Initial common Pb compositions of apatite and rutile were corrected by using the Pb isotopic composition of leached coexisting feldspar (Table DR2[1]). Titanite data were corrected by using the isotopic composition of feldspars in a Western Fiordland Orthogneiss granulite (F03-61). Feldspar Pb isotopic determination was accomplished by handpicking 1–3 mg plagioclase fractions, sequentially leaching separates with 7*M* $HNO_3$, 6*M* HCl, and 1*M* HF, separating Pb using HBr anion-exchange

chemistry, and statically analyzing Pb in four Faraday cups. Ultimately, the $^{206}Pb/^{238}U$ dates calculated using the initial common Pb composition of coexisting leached feldspars differed little from those calculated using the standard method of correcting with the Stacey-Kramers (1975) model for terrestrial Pb evolution. The maximum effect was on an apatite fraction characterized by the lowest radiogenic Pb to common Pb ratio of the dataset (sample F03-1, analysis a1, Pb*/Pbc = 0.1). The date calculated using coexisting leached feldspars for the initial common Pb composition was 3.7 m.y. younger than the date calculated using the Stacey-Kramers model. In contrast, the effect on the rutile dates (sample F03-61) was ≤ 0.15 m.y.

**REFERENCES CITED**


Aleinikoff, J.N., Wintsch, R.P., Fanning, C.M., and Dorais, M.J., 2002, U-Pb geochronology of zircon and polygenetic titanite from the Glastonbury Complex, Connecticut, USA: an integrated SEM, EMPA, TIMS, and SHRIMP study: Chemical Geology, v. 188, p. 125-147.

Chamberlain, K.R., and Bowring, S.A., 2000, Apatite-feldspar U-Pb thermochronometer: A reliable, mid-range (~450°C), diffusion-controlled system: Chemical Geology, v. 172, p. 73-200.

Cherniak, D.J., 1993, Lead diffusion in titanite and preliminary results on the effects of radiation damage on Pb transport: Chemical Geology, v. 110, p. 177-194.

Cherniak, D.J., 2000, Pb diffusion in rutile: Contributions to Mineralogy and Petrology, v. 139, p. 198-207.

Cherniak, D.J., Lanford, W.A., and Ryerson, F.J., 1991, Lead diffusion in apatite and zircon using ion implantation and Rutherford Backscattering techniques: Geochimica et Cosmochimica Acta, v. 55, p. 1663-1673.

Cherniak, D.J., and Watson, E.B., 2001, Pb diffusion in zircon: Chemical Geology, v. 172, p. 5-24.

Cherniak, D.J., Watson, E.B., Grove, M., and Harrison, T.M., 2004, Pb diffusion in monazite: A combined RBS/SIMS study: Geochimica et Cosmochimica Acta, v. 68, p. 829-840.

Dodson, M.H., 1973, Closure temperature in cooling geochronological and petrological systems: Contributions to Mineralogy and Petrology, v. 40, p. 259-274.

Frost, B.R., Chamberlain, K.R., and Schumacher, J.C., 2000, Sphene (titanite): phase relations and role as a geochronometer: Chemical Geology, v. 172, p. 131-148.

Hanson, G.N., Catanzaro, E.J., and Anderson, D.H., 1971, U-Pb ages for sphene in a contact metamorphic zone: Earth and Planetary Science Letters, v. 12, p. 231-237.

Krogstad, E.J. and Walker, R.J., 1994, Higher closure temperatures of the U-Pb system in large apatites from the Tin Mountain pegmatite , Black Hills, South Dakota, USA: Geochimica et Cosmochimica Acta, v. 58, p. 3845-3853.

Mezger, K., Hanson, G.N., and Bohlen, S.R., 1989, High-precision U-Pb ages of metamorphic rutile: application to the cooling history of high-grade terranes: Earth and Planetary Science Letters, v. 96, p. 106-118.

Stacey, J.S. and Kramers, J.D., 1975, Approximation of terrestrial lead isotope evolution by a two-stage model: Earth and Planetary Science Letters, v. 26, p. 207-221.

Verts, L.A., Chamberlain, K.R., and Frost, C.D., 1996, U-Pb sphene dating of contact metamorphism: the importance of sphene growth in the contact aureole of the Red Mountain pluton, Laramie Mountains, Wyoming: Contributions to Mineralogy and Petrology, v. 125, pl. 186-199.

Figure DR1. U-Pb concordia diagrams showing (A) F03-72 titanite, (B) F03-76 titanite, and (C) P69120 titanite.

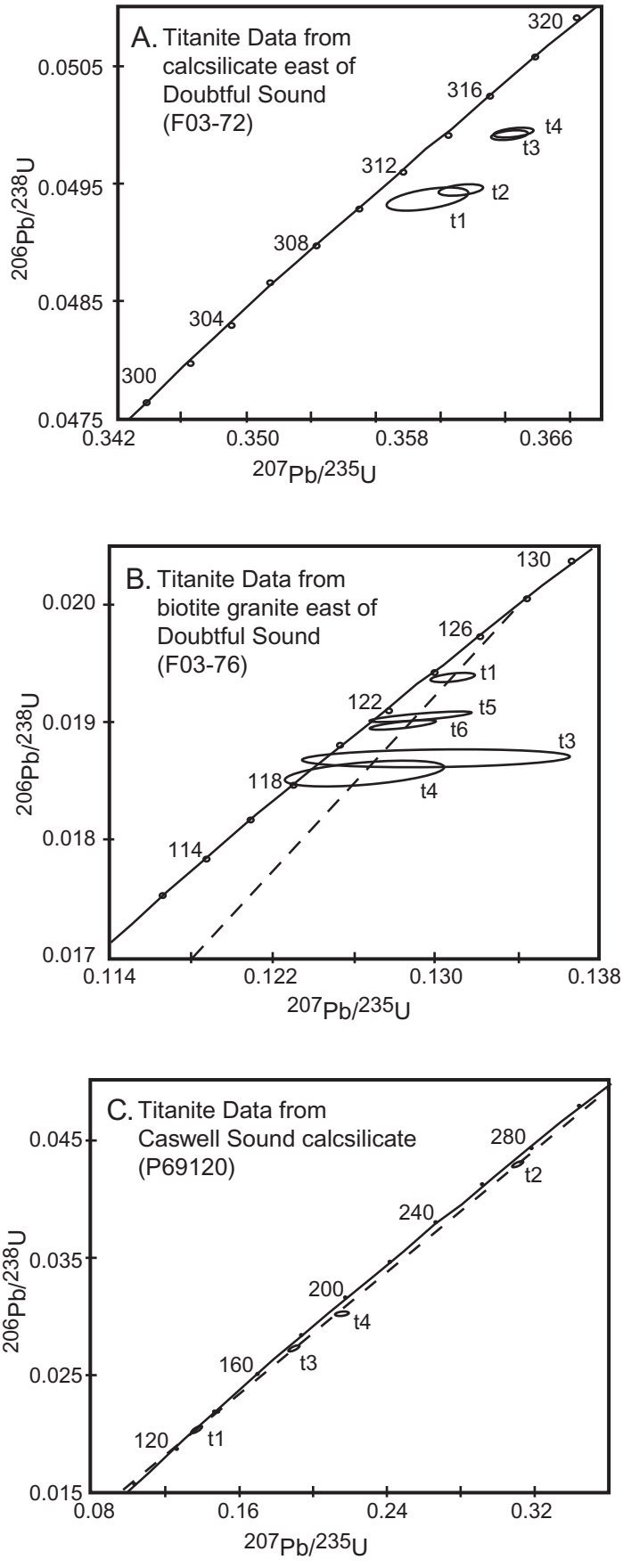


Figure DR1
Flowers et al.

Table DR1. U-Pb isotopic data for titanite, apatite, and rutile

| | | Composition | | | | | | Isotopic Ratios | | | | | | | | Dates (Ma) | | | |
|---|---|---|---|---|---|---|---|---|---|---|---|---|---|---|---|---|---|---|---|
| | | Wt | U | Pb | Th[c] | Pb*[d] | Pbc[d] | $^{206}Pb$[e] | $^{208}Pb$[f] | $^{206}Pb$[f] | | $^{207}Pb$[f] | | $^{207}Pb$[f] | | $^{206}Pb$[h] | $^{207}Pb$[h] | $^{207}Pb$[h] | corr. |
| Fr | #[a] | (µg)[b] | (ppm) | (ppm) | U | Pbc | (pg) | $^{204}Pb$ | $^{206}Pb$ | $^{238}U$ | % err[g] | $^{235}U$ | % err[g] | $^{206}Pb$ | % err[g] | $^{238}U$ | $^{235}U$ | $^{206}Pb$ | coef. |
| F03-55: Calcsilicate gneiss, Doubtful Sound (B43, 2040221E, 5523713N)[i] (P69539)[j] - yellow, flat, metamorphic titanite[k] | | | | | | | | | | | | | | | | | | | |
| t1 | 4 | 70 | 463.3 | 11.1 | 1.5 | 22.2 | 33.9 | 1089.6 | 0.483 | 0.01755 | (.08) | 0.11703 | (.11) | 0.04838 | (.07) | **112.1** | 112.4 | 117.6 | 0.761 |
| t2 | 4 | 30 | 681.2 | 15.1 | 1.1 | 21.2 | 20.5 | 1140.3 | 0.350 | 0.01760 | (.07) | 0.11735 | (.10) | 0.04836 | (.07) | **112.5** | 112.7 | 117.1 | 0.692 |
| t4 | 1 | 8 | 563.6 | 12.4 | 0.8 | 7.5 | 12.3 | 442.0 | 0.269 | 0.01750 | (.19) | 0.11608 | (.35) | 0.04811 | (.28) | **111.8** | 111.5 | 104.8 | 0.587 |
| t5 | 8 | 15 | 369.9 | 8.2 | 0.7 | 5.6 | 18.5 | 343.2 | 0.235 | 0.01739 | (.16) | 0.11589 | (.40) | 0.04834 | (.35) | **111.1** | 111.3 | 116.0 | 0.491 |
| t6 | 1 | 8 | 281.5 | 7.7 | 1.9 | 7.7 | 7.4 | 364.0 | 0.605 | 0.01764 | (.36) | 0.11748 | (.49) | 0.04831 | (.31) | **112.7** | 112.8 | 114.4 | 0.775 |
| t7 | 6 | 6 | 287.2 | 6.6 | 1.1 | 6.2 | 5.8 | 351.2 | 0.342 | 0.01738 | (.48) | 0.11609 | (.59) | 0.04845 | (.33) | **111.1** | 111.5 | 121.5 | 0.832 |
| F03-59C: Basement gneiss, Doubtful Sound (B43, 2041815E, 5521723N) (P69543) - brown, anhedral titanite | | | | | | | | | | | | | | | | | | | |
| t1 | 6 | 54 | 109.3 | 3.1 | 1.7 | 5.1 | 28.0 | 256.8 | 0.537 | 0.01767 | (.14) | 0.11799 | (.27) | 0.04844 | (.22) | **112.9** | 113.3 | 120.6 | 0.583 |
| t3 | 10 | 28 | 105.2 | 3.4 | 1.5 | 2.3 | 29.8 | 129.2 | 0.482 | 0.01754 | (.26) | 0.11701 | (.64) | 0.04839 | (.56) | **112.1** | 112.4 | 118.4 | 0.494 |
| t4 | 3 | 30 | 77.6 | 2.4 | 2.0 | 4.5 | 13.4 | 215.9 | 0.655 | 0.01775 | (.34) | 0.11840 | (.58) | 0.04837 | (.44) | **113.4** | 113.6 | 117.3 | 0.642 |
| t5 | 12 | 18 | 292.9 | 8.5 | 1.8 | 5.8 | 22.7 | 280.5 | 0.592 | 0.01765 | (.16) | 0.11782 | (.25) | 0.04842 | (.19) | **112.8** | 113.1 | 119.7 | 0.658 |
| F03-61: Western Fiordland Orthogneiss granulite, Doubtful Sound (B43, 2041326E, 5519055N) (P69549) - dark red, tabular, euhedral rutile | | | | | | | | | | | | | | | | | | | |
| r1 | 6 | 112 | 14.6 | 0.3 | 0.0 | 0.8 | 22.4 | 72.4 | 0.000 | 0.01152 | (.69) | 0.07597 | (1.31) | 0.04782 | (1.06) | **73.9** | 74.4 | 90.2 | 0.586 |
| r4 | 3 | 255 | 12.7 | 0.3 | 0.0 | 0.9 | 34.9 | 81.8 | 0.000 | 0.01071 | (.35) | 0.07113 | (.89) | 0.04816 | (.79) | **68.7** | 69.8 | 107.0 | 0.484 |
| r5 | 4a | 300 | 9.4 | 0.2 | 0.0 | 1.0 | 26.4 | 89.8 | -0.001 | 0.01040 | (.41) | 0.06797 | (.75) | 0.04741 | (.60) | **66.7** | 66.8 | 69.8 | 0.609 |
| r6 | 6a | 135 | 23.2 | 0.4 | 0.0 | 1.2 | 23.9 | 104.5 | -0.001 | 0.01026 | (.81) | 0.06718 | (1.09) | 0.04749 | (.69) | **65.8** | 66.0 | 73.9 | 0.772 |
| F03-72: Calcsilicate, east of Doubtful Sound (C43, 2055994E, 5507278N) (P69562) - yellowish-brown titanite | | | | | | | | | | | | | | | | | | | |
| t1 | 1 | 95 | 94.2 | 10.1 | 2.5 | 3.3 | 224.4 | 145.5 | 0.854 | 0.04991 | (.06) | 0.36624 | (.26) | 0.05322 | (.25) | **310.6** | 313.1 | 331.7 | 0.407 |
| t2 | 3 | 54 | 105.3 | 12.1 | 3.0 | 3.4 | 147.0 | 141.8 | 1.011 | 0.04992 | (.07) | 0.36644 | (.29) | 0.05324 | (.27) | **311.1** | 314.6 | 340.4 | 0.418 |
| t3 | 6 | 33 | 118.4 | 13.2 | 3.5 | 6.1 | 61.7 | 218.4 | 1.197 | 0.04945 | (.09) | 0.36321 | (.29) | 0.05327 | (.26) | **314.0** | 316.9 | 338.2 | 0.443 |
| t4 | 7 | 23 | 70.3 | 10.0 | 4.2 | 2.8 | 59.9 | 102.3 | 1.434 | 0.04936 | (.17) | 0.36118 | (.56) | 0.05307 | (.51) | **314.0** | 317.0 | 339.0 | 0.450 |
| F03-76: Biotite granite, east of Doubtful Sound (C43, 2063139E, 5505134N) (P69565) - dark brown titanite | | | | | | | | | | | | | | | | | | | |
| t1 | 1 | 165 | 31.8 | 2.6 | 7.8 | 2.7 | 114.8 | 75.1 | 2.508 | 0.01937 | (.13) | 0.13080 | (.68) | 0.04897 | (.64) | **123.7** | 124.8 | 146.3 | 0.421 |
| t3 | 1 | 145 | 9.3 | 0.8 | 2.3 | 0.5 | 81.7 | 38.4 | 0.769 | 0.01869 | (.33) | 0.13003 | (4.11) | 0.05045 | (4.05) | **119.4** | 124.1 | 215.9 | 0.217 |
| t4 | 8 | 60 | 12.7 | 1.4 | 5.1 | 0.6 | 54.2 | 35.4 | 1.662 | 0.01857 | (.53) | 0.12650 | (2.52) | 0.04942 | (2.34) | **118.6** | 120.9 | 167.7 | 0.425 |
| t5 | 1 | 245 | 34.9 | 2.6 | 3.9 | 1.1 | 303.8 | 52.9 | 1.262 | 0.01904 | (.16) | 0.12921 | (1.59) | 0.04922 | (1.50) | **121.6** | 123.4 | 158.5 | 0.596 |
| t6 | 1 | 280 | 28.5 | 2.2 | 5.6 | 1.5 | 254.0 | 56.7 | 1.810 | 0.01899 | (.10) | 0.12833 | (.98) | 0.04901 | (.93) | **121.3** | 122.6 | 148.3 | 0.550 |

Table DR1. (continued)

| | | Composition | | | | | | Isotopic Ratios | | | | | | | | Dates (Ma) | | | |
|---|---|---|---|---|---|---|---|---|---|---|---|---|---|---|---|---|---|---|---|
| | | Wt | U | Pb | Th[c] | Pb*[d] | Pbc[d] | $^{206}Pb$[e] | $^{208}Pb$[f] | $^{206}Pb$[f] | | $^{207}Pb$[f] | | $^{207}Pb$[f] | | $^{206}Pb$[h] | $^{207}Pb$[h] | $^{207}Pb$[h] | corr. |
| Fr | #[a] | (µg)[b] | (ppm) | (ppm) | U | Pbc | (pg) | $^{204}Pb$ | $^{206}Pb$ | $^{238}U$ | % err[g] | $^{235}U$ | % err[g] | $^{206}Pb$ | % err[g] | $^{238}U$ | $^{235}U$ | $^{206}Pb$ | coef. |
| OU49124: Mafic granulite, Milford Sound (D40, 2097450E, 5592000N) - dark brown, irregular titanite | | | | | | | | | | | | | | | | | | | |
| t1 | 1 | 145 | 79.2 | 6.0 | 2.4 | 0.6 | 538.4 | 44.2 | 0.751 | 0.01877 | (.10) | 0.12362 | (1.39) | 0.04776 | (1.34) | **119.9** | 118.3 | 87.5 | 0.602 |
| t2 | 1 | 145 | 66.5 | 3.9 | 1.2 | 0.7 | 340.0 | 52.7 | 0.379 | 0.01881 | (.09) | 0.12781 | (.92) | 0.04927 | (.88) | **120.1** | 122.1 | 160.9 | 0.560 |
| t3 | 1 | 70 | 65.3 | 3.9 | 1.6 | 0.7 | 161.6 | 52.5 | 0.531 | 0.01874 | (.14) | 0.12699 | (1.21) | 0.04915 | (1.15) | **119.7** | 121.4 | 155.0 | 0.501 |
| t4 | 1 | 70 | 49.2 | 4.2 | 2.3 | 0.5 | 197.0 | 39.5 | 0.768 | 0.01865 | (.18) | 0.12831 | (1.93) | 0.04990 | (1.83) | **119.1** | 122.6 | 190.4 | 0.589 |
| P69120: Calcsilicate gneiss, Caswell Sound (B41, 2048747E, 5560266N) - light brown titanite | | | | | | | | | | | | | | | | | | | |
| t1 | 1 | 13 | 46.6 | 2.0 | 1.1 | 1.1 | 12.8 | 77.5 | 0.352 | 0.02024 | (1.00) | 0.13622 | (1.38) | 0.04882 | (.90) | **129.2** | 129.7 | 139.1 | 0.756 |
| t2 | 1 | 17 | 49.0 | 4.0 | 0.5 | 1.2 | 31.5 | 91.3 | 0.175 | 0.04293 | (.34) | 0.31062 | (.64) | 0.05247 | (.51) | **271.0** | 274.7 | 306.0 | 0.596 |
| t3 | 2 | 23 | 29.2 | 2.0 | 1.2 | 0.9 | 24.7 | 66.1 | 0.404 | 0.02732 | (.60) | 0.19210 | (1.07) | 0.05100 | (.84) | **173.8** | 178.4 | 240.7 | 0.623 |
| t4 | 2 | 23 | 33.3 | 2.3 | 0.2 | 0.7 | 31.4 | 65.8 | 0.120 | 0.03024 | (.48) | 0.21797 | (1.32) | 0.05229 | (1.17) | **192.0** | 200.2 | 297.9 | 0.477 |
| F03-1A: Darran Complex diorite, east of Milford Sound (D40, 2114889E, 5591239N) (P69478) | | | | | | | | | | | | | | | | | | | |
| a1 | 13 | 115 | 6.2 | 2.2 | 2.8 | 0.1 | 226.8 | 22.8 | 0.996 | 0.02033 | (.45) | 0.15018 | (6.94) | 0.05357 | (6.58) | **129.8** | 142.1 | 352.9 | 0.820 |
| a2 | 11 | 125 | 9.8 | 2.3 | 2.5 | 0.2 | 254.7 | 24.6 | 0.934 | 0.01949 | (.33) | 0.15113 | (4.75) | 0.05625 | (4.48) | **124.4** | 142.9 | 462.4 | 0.810 |
| a3 | 13 | 75 | 8.2 | 2.1 | 2.7 | 0.2 | 135.1 | 24.5 | 0.925 | 0.02001 | (.43) | 0.14520 | (5.46) | 0.05262 | (5.16) | **127.7** | 137.7 | 312.5 | 0.699 |
| a4 | 13 | 46 | 15.9 | 3.8 | 2.8 | 0.2 | 153.7 | 24.7 | 0.914 | 0.02002 | (.42) | 0.14001 | (5.83) | 0.05073 | (5.52) | **127.8** | 133.1 | 228.5 | 0.755 |
| a5 | 14 | 50 | 8.1 | 2.1 | 2.7 | 0.2 | 90.5 | 24.4 | 1.000 | 0.02021 | (.63) | 0.15618 | (7.51) | 0.05604 | (7.11) | **129.0** | 147.4 | 454.2 | 0.658 |

[a] Number of grains in fraction, a indicates the fraction was abraded

[b] Sample weights were estimated to within 40% using measured grain dimensions and a nominal density of 3.5 g/cm$^3$ for titanite, 3.2 g/cm$^3$ for apatite, and 4.2 g/cm$^3$ for rutile.

[c] Th contents calculated from radiogenic $^{208}Pb$ and the $^{207}Pb/^{206}Pb$ date of the sample, assuming concordance between U-Th-Pb systems.

[d] Pb* and Pbc represent radiogenic Pb and common Pb respectively.

[e] Measured ratio corrected for fractionation and spike contribution; Pb fractionation was 0.12 ±0.04%/a.m.u. for Faraday detector or 0.2 ± 0.04%/a.m.u. for Daly detector analysis, based on daily analysis of NBS-981.

[f] Measured ratios corrected for fractionation, spike, blank, and initial common Pb; nominal U blank = 0.1 pg ± 50% (2s); nominal Pb blank = 2.0 pg ± 50% for titanite, apatite and rutile (2s) or where lower, the total common Pb of the analysis ±10% (2s); measured laboratory Pb composition: $^{206}Pb/^{204}Pb$ = 19.10, $^{207}Pb/^{204}Pb$ = 15.72, $^{208}Pb/^{204}Pb$ = 38.65 ± 0.01 (2s); initial Pb composition from leached feldspars.

[g] Numbers in parentheses are the % errors reported at the 2s confidence interval, propagated using the algorithms of Ludwig (1980).

[h] Isotopic ages calculated using the decay constants of Jaffey et al. (1971): $\lambda(^{235}U) = 9.8485 \times 10^{-10}$ yr$^{-1}$ and $\lambda(^{238}U) = 1.55125 \times 10^{-10}$ yr$^{-1}$; error in $^{207}Pb/^{206}Pb$ date reported at the 2s confidence interval. Dates in bold are the best age estimates.

[i] UTM coordinates for each sample given in New Zealand map grid reference

[j] For samples with a second sample number, a similar, but not identical, sample from the same outcrop is available through the NZ PETLAB database.

[k] Description of analyzed grains

Table DR2. Pb isotopic composition of leached feldspar separates

| sample[a] | wt (mg) | $\frac{^{206}Pb}{^{204}Pb}$[b] | $\frac{^{207}Pb}{^{204}Pb}$ | $\frac{^{208}Pb}{^{204}Pb}$ |
|---|---|---|---|---|
| F03-61: WFO | | | | |
| Fsp1 | 2.30 | 18.669 | 15.604 | 38.508 |
| Fsp2 | 1.40 | 18.666 | 15.608 | 38.496 |
| F03-1A: Darran Complex | | | | |
| Fsp1 | 1.70 | 18.662 | 15.624 | 38.455 |
| Fsp2 | 1.60 | 18.622 | 15.621 | 38.404 |

[a] Least radiogenic leach from each feldspar fraction

[b] Standard error on analyses is less than 0.033.

Pb fractionation is 0.12 ±0.04%/a.m.u. for Faraday detector based on daily analysis of NBS-981.